Chemical Engineering & Processing: Process Intensification 158 (2020) 108169

Contents lists available at ScienceDirect

Chemical Engineering and Processing - Process Intensification

journal homepage: www.elsevier.com/locate/cep

Analysis of the effective thermal conductivity of isotropic and anisotropic Periodic Open Cellular Structures for the intensification of catalytic processes

Mauro Bracconi, Matteo Ambrosetti, Matteo Maestri, Gianpiero Groppi, Enrico Tronconi *

Laboratory of Catalysis and Catalytic Processes, Dipartimento di Energia, Politecnico di Milano, via La Masa 34, Milano, Italy

ARTICLE INFO

Keywords:
Heat transfer
POCS
Catalyst supports
Process intensification
3D printing

ABSTRACT

Conductive metallic Periodic Open Cellular Structures (POCS) are considered a promising solution for the intensification of heat-transfer limited catalytic processes thanks to their enhanced thermal conductivity. Herein, the heat conduction in the solid matrix has been investigated through 3D numerical simulations. The porosity together with the intrinsic conductivity of the material have a major effect on the effective thermal conductivity, while a negligible influence of the cell shape and size is found. A correlation previously derived for the description of open cell foams shows an excellent agreement with the results of POCS structures.

POCS are produced by additive manufacturing, e.g. 3D printing, providing degrees of freedom in the geometry design. Anisotropic cubic cell structures have been investigated for the first time to explore the possibility to promote or decrease preferentially the heat conduction in the radial or the axial direction. At constant solid fraction and cell size, these structures can improve the effective thermal conductivity of the solid matrix up to 40 % and 100 % for structures thickened in two or one direction respectively. This concept paves the way to the design of metamaterials with tailored properties, granting additional degrees of freedom for the intensification of heat-transfer limited catalytic processes.

1. Introduction

Operation and design of reactors for many energy-intensive catalytic processes depend on their heat exchange capacity, which makes the enhancement of the heat transfer efficiency one of the most relevant routes for process intensification [1,2].

Multi-tubular packed beds are often employed for strongly exothermal reactions, such as selective oxidations [3] and hydrogenations [4], or for endo-thermal processes like steam reforming [5]. A poor heat transfer between the reactor and the heating/cooling medium may cause excessive temperature gradients in the radial and axial direction, with loss of activity and selectivity. Besides, in the case of an exothermal reactions, the formation of hotspots may lead to catalyst deactivation and thermal runaway [6]. Heat transfer in packed beds is granted by heat conduction, through the catalytic pellets, convection in the fluid phase and radiation [7,8]. However, packed beds are characterized by a poor static heat conduction, since this mechanism is limited by pellet-to-pellet or pellet-to-wall random contacts. Hence, packed bed systems mainly rely on convective heat transfer, that is enhanced by operating the reactor at high specific mass flow rates [9]. To ensure a sufficient contact time, such an operation mode poses design constraints on the length of the reactor tubes, making the intensification of these reactors extremely difficult.

Structured catalyst carriers have been proposed in the last decade to overcome heat transfer limitations in tubular reactors [10]. Different structures have been proposed for the intensification of catalytic processes, including wire meshes [11], structured packings, open cross flow structures [12], metallic washcoated and packed honeycombs [3,13] and, more recently, open cell foams [14]. These supports may be produced in ceramic or metallic materials. The former ones are poorly conductive, therefore the heat transfer is mainly associated with convection in the gas phase and with radiation in case of high temperatures applications [15,16]. Instead, when they are manufactured with conductive metals, the heat transfer performance is mainly associated with the thermal conduction in their solid matrix [17], which grants flow-independent performances and becomes the dominant contribution to the overall heat transfer [18,19]. The open cell foams, in particular, are considered one of the most promising options to intensify

* Corresponding author.
E-mail address: enrico.tronconi@polimi.it (E. Tronconi).

https://doi.org/10.1016/j.cep.2020.108169
Received 6 August 2020; Received in revised form 22 September 2020; Accepted 5 October 2020
Available online 10 October 2020

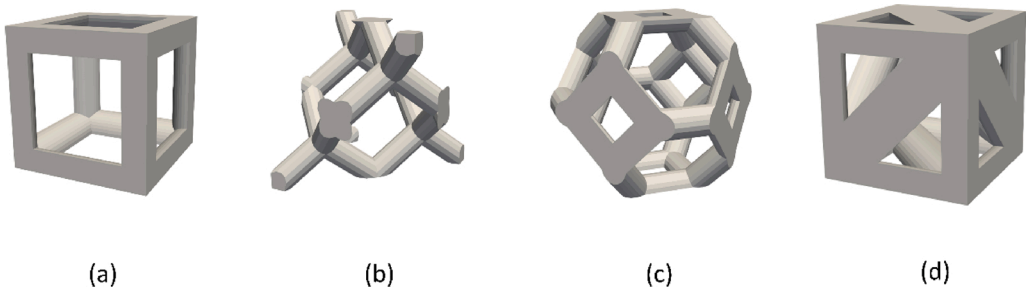

Fig. 1. Unit cells considered for the analysis: cubic (a), diamond (b), TKKD (c) and FCC (d).

heat-transfer limited processes since the interconnected solid matrix grants high effective thermal conductivities [20], enabling at the same time an efficient radial and axial mass transport through the open pores combined with low pressure drop.

Structured supports are usually activated by washcoating [21], which however limits the catalyst inventory to 20 % of the reactor volume at best, i.e. much less than the catalyst loading of conventional packed beds. To overcome such a limitation, Tronconi and co-workers proposed the concept of packed foams [22] where the catalytic pellets are loaded in the open pores of the foam structure. This enables to achieve high catalyst loadings [23] while maintaining the enhanced heat transfer performances due to the presence of the continuous conductive support embedded in the packed bed [18,24,25].

The potential of structured supports for heat transfer enhancement is not confined to open-cell foams but, in principle, is retained by every structure which simultaneously exhibits an interconnected solid matrix along with an open cellular geometry. In this view, Freund and co-workers [26,27] proposed the concept of Periodic Open Cellular Structures (POCS). They consist in a collection of repeated elementary cells in the three spatial directions, resulting in perfectly ordered and regular structures. Plenty of unit cells with different geometries are available, as shown in Fig. 1, from the simple cubic and face centered cubic (FCC) cells to more complex diamond and tetrakaidekahedral (TKKD) cells. Many others can be developed according to specific process requirements showing an unprecedent degree of freedom for the advanced design of chemical reactors. These structures combine a regular geometry with high surface area, low pressure drop and high effective thermal conductivity due to the totally interconnected solid matrix [27,28]. POCS can be nowadays easily manufactured via additive manufacturing methods and are a promising alternative to open-cell foams to intensify energy intensive processes. Structures with great geometrical flexibility can now be produced with conductive metals thanks to modern 3D printing techniques such as Selective Electron Beam Melting (SEBM) [28], Selective Laser Melting (SLM) [29] or Selective Laser Sintering (SLS), enabling their facile manufacturing in a variety of shapes and sizes. Moreover, 3D printing shows a great potential also in the analysis and investigation of transport properties of cellular materials, such as open cell foams [30] and POCS. A combination of numerical simulations on virtual models and experiments on 3D printed replicas can greatly facilitate the development of engineering correlations and design guidelines.

Recently, POCS have been studied as efficient catalyst supports due to their improved heat transfer properties. Grande and coworkers [31,32] studied the heat transfer in 3D printed cubic cell structures, manufactured in AlSi10, for the intensification of catalytic NO oxidation in nitric acid production. Based on non-reactive heat transfer tests, they investigated the effect of the geometry on the overall heat transfer, which ranges $800 - 2000\ W\ m^{-2}\ K^{-1}$ mainly due to the presence of the interconnected solid matrix. Danaci et al. [33] employed 3D printed stacked structures (3DFD) manufactured in copper and stainless steel for the intensification of CO_2 methanation thanks to the improved temperature control in the reactor ensured by the conductive structure. Fratalocchi et al. [34] demonstrated the superior heat management in the strongly exothermic Fischer-Tropsch synthesis by comparing POCS with open cell foams as reactor internals in packed bed. They showed that packed POCS allows for higher CO conversions per pass (up to 80 %) while avoiding thermal runaway, reaching performances impossible for a packed bed working in the same conditions.

A quantification of the overall heat transport properties of these structures was performed by Busse et al. [27] through dedicated heat transfer tests under non-reacting flow conditions. Focusing on cubic cells, engineering correlations for the description of the convective and wall heat transfer coefficients were developed based on empirical observations. Recently, Ambrosetti et al. [35] have performed an experimental assessment of the heat transport properties of packed POCS aiming at the development of an heat transfer model for these systems. Once again, the analyses carried out on different manufacturing materials reveal a strong dependency of the overall heat transfer performances on the thermal conductivity in the solid matrix.

As documented by literature, the thermal conductivity of the solid matrix of structured substrates plays a major role in determining the overall heat transfer performances in reacting and non-reacting systems. Hence, engineering quantification of the effective thermal conductivity of these structures is of utmost importance to enable a rational reactor design. Even if some methods for the measurements of the thermal conductivity are available (i.e. laser flash methods [36]), the direct measurement of this property is not trivial for macro-porous highly conductive structures, therefore the effective thermal conductivity is usually indirectly obtained from global heat transfer measurements [37]. Conversely, numerical 3D simulations can be directly employed to investigate the intrinsic performances of the solid matrix. In doing so, it is possible to directly determine the thermal conductivity of the solid structure, to perform sensitivity analyses of the structure properties and to develop engineering correlations for this crucial property. In fact, the same approach has been already employed for the analysis of open-cell foams. Several authors performed numerical simulations over μ-CT scans of open-cell foams to determine the structure thermal conductivity [38,39], whereas Randrianalisoa et al. performed simulations over virtual-reconstructed open-cell foams [40]. Bracconi et al. [20] reported a systematic study of the effective thermal conductivity of synthetic foams structures, which addressed the effects of the main geometrical parameters (porosity, cell size and node-to-strut ratio), leading to the derivation of a theoretically grounded correlation for the effective thermal conductivity. Open cell foams are intrinsically characterized by a random structure with a distribution of cell, pore and strut sizes [41]. Moreover, these structures are characterized by convex parabolic strut profiles that limit the thermal conductivity, as clearly demonstrated by our previous work on virtually generated foams with different strut geometries [20].

The first numerical study on the effective thermal conductivity of POCS was reported by Bianchi et al. [42], who investigated both two unit cells (e.g. cubic and TKKD) and different strut cross sectional shapes in a range of void fractions from 0.75 to 0.95. First, the analysis revealed a quasi-negligible influence of the strut cross-sectional shape on the

Table 1
Analytical relationships between cell size (d_c), strut diameter (d_s) and the void fraction (ε).

Cubic [44]	FCC
$\varepsilon = 1 - \frac{\frac{3(d_c - d_s)d_s^2\pi}{4} + \left(\frac{3}{4}\pi - \sqrt{2}\right)d_s^3}{d_c^3}$	$\varepsilon = 1 - \frac{\left(\frac{3}{4}\pi - \sqrt{2}\right)d_s^3 + \frac{3}{4}\left(\left(\sqrt{2}+1\right)d_c - (\sqrt{2}+2)\,d_s\right)d_s^2\pi}{d_c^3}$
TKKD [20]	**Diamond** [28]
$\gamma = \frac{1}{2}\text{acos}\left(-\frac{1}{3}\right)$ $\quad d_n = \frac{d_s}{\sin(\gamma)}$ $\quad h_n = 1 - \cos(\gamma)$ $\quad \varepsilon = 1 - \frac{2\pi d_n^3\left(1 - 3h_n^2 + h_n^3\right) + 6\pi d_s^2\left(\frac{\sqrt{2}}{4}d_c - d_n\cos(\gamma)\right)}{d_c^3}$	$\varepsilon = 1 - \frac{3\sqrt{3}\pi}{16\left(\frac{d_c\sqrt{3}}{4\,d_s}\right)^3}\left(\frac{d_c\sqrt{3}}{4\,d_s} + \frac{\sqrt{2}}{2}\left(\frac{1}{3} - \frac{\sqrt{3}}{2}\right)\right)$

effective thermal conductivity which is observable only at low void fractions. Moreover, the authors investigated the effect of different distributions of solid material along the strut by computing the heat transfer performances for different ratios between node diameter and the strut diameter at the mid length. In full analogy with foams, they observed that an increment of the ratio reduces the effective thermal conductivity. Finally, a negligible effect of the two different cell shapes was recovered resulting in the development of an empirical correlation for the effective thermal conductivity of these structures.

In view of the great potential of POCS structures for the intensification of heat transfer in energy-intensive catalytic reactors, a fundamental investigation of the effective thermal conductivity is crucial for their adoption in industrially relevant systems.

In this work, we present a systematic investigation of the effective thermal conductivity in the solid matrix using numerical simulations for several unit cells (cubic, diamond, TKKD, FCC) on a broad range of void fractions and cell sizes, aiming at extending and generalizing the work of Bianchi et al. [42]. In this view, a wide range of porosities (from 0.65 to 0.97) and cell shapes has been considered while addressing the influence of the cell size. Our analysis reveals that the thermal conductivity strongly depends on the void fraction, whereas the performances are almost cell-independent, apart from minor deviations.

Conventional POCS unit cells are isotropic (i.e. show the same property in all the directions of the space), therefore, it is not possible to design structures that show different properties in the three spatial directions, which limits the optimization of these structures. A possibility to introduce additional degrees of freedom in their design is the adoption of anisotropic elementary cells. In this work, we also propose, to the best of our knowledge, for the first time in literature, the concept of anisotropic POCS aiming at a selective tuning of the thermal conductivity performances in a specific (axial or radial) direction. As a matter of fact, several catalytic processes may benefit from either an enhanced radial conductivity (e.g. externally heated or cooled reactors) [1] or an enhanced axial conductivity (e.g. Lumped Thermal Reactors) [43]. Herein, we quantify the performances of anisotropic POCS by considering a cubic unit cell, since its simple geometry readily enables a topological optimization aimed at enhancing/decreasing the thermal conductivity in a given direction. As a result, we find that anisotropic structures, at fixed porosity, can increase the effective heat conductivity up to 40 % and 100 % for structures thickened in two or one direction, thus providing one additional degree of freedom for the design of optimized catalytic reactors.

2. Methods and models

In this section, we briefly describe the procedure for the generation of the virtual POCS model required for the numerical simulation of the thermal conduction in the solid matrix along with the details of the meshing procedure. Then, we introduce the equations adopted for the evaluation of the stagnant thermal conductivity of the solid matrix.

2.1. POCS generation

The numerical analysis of the thermal conduction in the solid matrix requires the generation of a representative computational domain of the POCS structure.

The three-dimensional structures are generated by the repetition of the unit cell in the three spatial directions. In this work, we consider different unit cells, i.e. cubic, diamond, TKKD, face centered cubic (FCC), respectively, as shown in Fig. 1. FCC is a cubic-like structure with additional ligaments in diagonal position on the faces of the structure.

The cell size (d_c), the strut size (d_s) and the porosity (ε) of these structures are linked by characteristic relationships. The geometrical correlations proposed in the literature for cubic, diamond, TKKD cells [20,28,44] are reported in Table 1 together with the correlation for the FCC cell, which is developed in this work as described in the Appendix A1. These correlations are herein adopted to compute the strut diameter, required to generate the virtual structures, by starting from the cell diameter and the porosity, which are selected as primary design parameters.

The generation of the tridimensional structures required for the numerical analysis is carried out by means of OpenSCAD, a parametric CAD software.

2.2. Numerical simulation of heat conduction in the solid structure

The temperature distribution in the three-dimensional POCS domain is computed by solving the steady-state Laplace equation, Eq. (1).

$$k_s \nabla^2 T = 0 \tag{1}$$

where T is the temperature in the solid matrix and k_s is the intrinsic thermal conductivity of the solid material, which is assumed to be constant in this work.

A temperature gradient is imposed between two opposite faces of the computational domain along the considered axis. All the other surfaces are considered adiabatic.

Eq. (1) is solved by the finite volume method implemented in the OpenFOAM framework [45]. A second order discretization scheme is employed for the Laplacian operator and the simulations are assumed to converge when the temperature residual is below 10^{-10}.

The thermal conduction through the solid matrix is quantified in terms of mono-directional stagnant effective thermal conductivity (k_{eff}) computed according to Eq. (2).

$$k_{eff} = \frac{-L\int_A J\, dA}{\Delta T\, S} \tag{2}$$

where J is the heat flux obtained from the simulation, A is the actual area of the POCS where the temperature is imposed, S and L are the area of the face and the thickness of the computational domain, ΔT is the temperature difference imposed in the considered direction.

A proper meshing procedure is pivotal for the faithful description of the transport properties. The computational domain for the solid phase is generated from a CAD file of the POCS, in turn obtained by means of

Table 2
Dimensionless effective thermal conductivity for three different directions for cubic ($\varepsilon = 0.835$ - $d_c = 3$ mm), diamond ($\varepsilon = 0.810$ - $d_c = 3$ mm), TKKD ($\varepsilon = 0.850$ - $d_c = 3$ mm) and FCC ($\varepsilon = 0.900$ - $d_c = 3$ mm) cells.

	k_{eff}/k_s [-]		
Structure	*x*	*y*	*z*
Cubic cell	0.07509	0.07509	0.07509
Diamond cell	0.08700	0.08648	0.08596
TKKD cell	0.06994	0.06994	0.06994
FCC cell	0.04102	0.04110	0.04105

the freeware CAD software OpenSCAD by a regular repetition of the single unit cell in the three-dimensional space. The computational domain is then built by employing the snappyHexMesh utility part of the OpenFOAM framework [45]. The utility starts from a uniform hexahedral background mesh, refines the region of the initial computational domain close to the CAD surface by means of the cut-cell methodology and, finally, snaps the mesh onto the CAD surface to obtain a body-fitting mesh. In this work, we employed a high-quality refinement (four levels) along the POCS surface. In doing this, the resulting computational domain exhibits all the details of the original CAD files. Mesh convergence has been carried out to obtain a domain independent solution of the target quantity, i.e. the effective thermal conductivity. Several background meshes with different mesh density have been tested. Herein, the computational domain is deemed to converge when the influence on the effective thermal conductivity is below 0.5 %. This is obtained by employing a background mesh for which the ratio between the strut diameter and the grid size is equal to 4. Additional details on the mesh convergence are reported in the Supplementary material.

The analysis of the transport properties in cellular materials requires the definition of a representative elementary volume (REV) suitable to describe the real structure behavior without any sample size effect on the calculation of the target transport property. POCS are regular and periodic structures for which the definition of REV is straightforward. The entire unit cell or even a cell portion [42] are intrinsically the representative elementary volume for the analysis related to the solid properties. In this work, we have numerically investigated structures consisting of 1, 3, 5, and 7 cells to span a large range of sample dimensions. The results are reported in the Supplementary material. As expected, the analysis revealed that one cell is enough to properly describe the stagnant effective thermal conductivity.

3. Results and discussion

A parametric analysis of the effect of different geometrical and topological parameters is performed. First, the effect of the direction is analyzed followed by the effect of cell size and solid fraction. Finally, a comparison between the performances of the unit cell shape is carried out.

3.1. Effect of direction

According to their periodically ordered structure, isotropic properties in the three space directions are expected for POCS obtained by the repetition of identical and isotropic unit cells Accordingly, we have hereby checked the proper choice of the unit cell geometry by evaluating the effective thermal conductivity along the three directions of the space for each elementary cell shown in Fig. 1. Results listed in Table 2 confirm that the effective thermal conductivity is independent of the direction, since the calculated values are the same along the three axes. This confirms that a correct unit cell (both in terms of geometry and physical properties) is effectively chosen for the calculations.

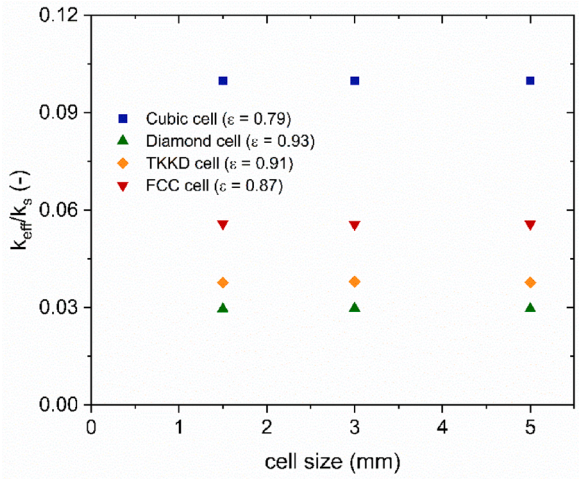

Fig. 2. Dimensionless effective thermal conductivity as a function of the cell diameter for diamond (green upward triangle), cubic (blue square), TKKD (orange diamond), FCC (red downward triangle) cells.

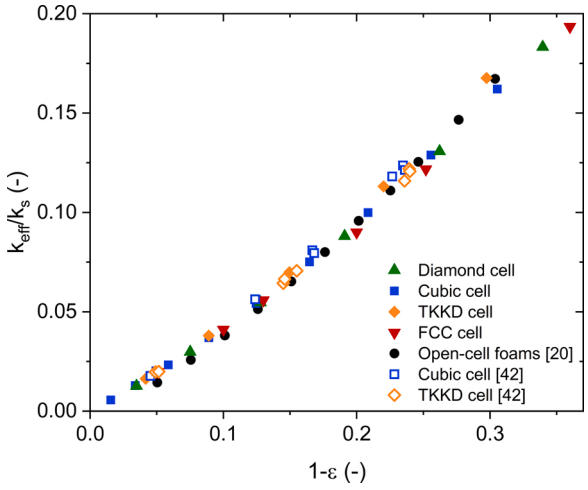

Fig. 3. Dimensionless effective thermal conductivity as a function of the solid fraction for diamond (green upward triangle), cubic (blue square), TKKD (orange diamond), FCC (red downward triangle) cells and open-cell foams [20] (black circle) along with numerical results from Bianchi et al. [42] for cubic (empty blue square) and TKKD (empty orange diamond) cells.

3.2. Effect of the cell size

The effect of cell size is investigated by parametrically changing the cell diameter in the range 1.5–5 mm with a constant void fraction.

The results are shown in Fig. 2. For any cell shape, once the void fraction is fixed, the effective thermal conductivity is not changing with the cell size. Hence, the effective thermal conductivity of the solid phase is practically independent of the cell diameter as already observed for open-cell foams [20].

3.3. Effect of the porosity

To investigate the effect of the porosity, several samples have been generated characterized by a broad range of different void fractions covering the interval between 0.65 and 0.97. Fig. 3 shows the effective thermal conductivity as a function of the solid fraction (i.e. the complement to one of the porosity) for all the unit cells investigated in this work.

The numerical simulations reveal that the solid fraction has a strong

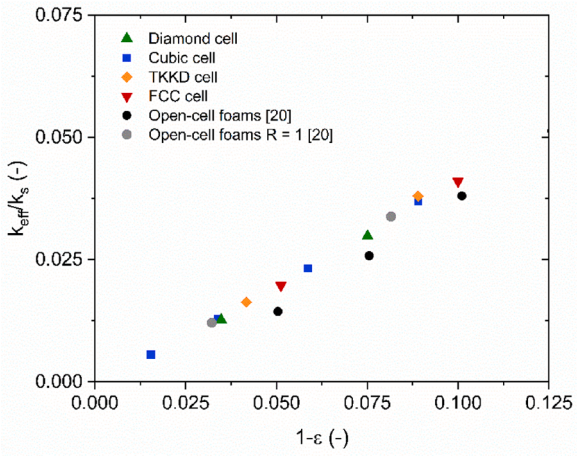

Fig. 4. Dimensionless effective thermal conductivity as a function of the solid fraction for POCS and for open-cell foams with constant strut (grey circle) and parabolic strut (black circle) [20].

effect on the effective thermal conductivity as also observed by Bianchi et al. [42], whose findings for cubic and TKKD cells are in excellent agreement with our calculations. The results highlight a slightly more than linear dependence on the solid fraction. In particular, an increment of the solid fraction determines an increase of the effective thermal conductivity. By keeping the cell diameter constant, indeed, an increment of the solid fraction has the effect to generate structures with larger strut diameters resulting in an improvement of the heat transfer efficiency. A similar behavior has been already reported in the literature for open-cell foams [20].

3.4. Effect of the elementary cell shape

Fig. 3 also shows the influence of the unit cell shape on the effective thermal conductivity. Interestingly, the effective thermal conductivity appears to be almost independent of the unit cell shape. This result confirms and extends the findings of Bianchi et al. [42], who observed the same behavior in the analysis of cubic and TKKD cells in a narrower range of porosities.

In the region of low solid fraction (1-ε < 0.12), the performances of the different POCS unit cells are perfectly superimposed one to the other, resulting in a negligible effect of the topology of the unit cell on the intrinsic heat transfer performances of the solid matrix. By increasing the solid fraction, the POCS shapes still show similar performances although some minor differences appear. In particular, TKKD cells provide the highest effective thermal conductivity, while the FCC cells show the poorest performances. This could be ascribed to an effect of the junction between struts which provides cell-specific heat transfer resistances. Nevertheless, the magnitude of the deviations is not significant (±7%) resulting in comparable performances of all the POCS in the entire range of solid fraction investigated.

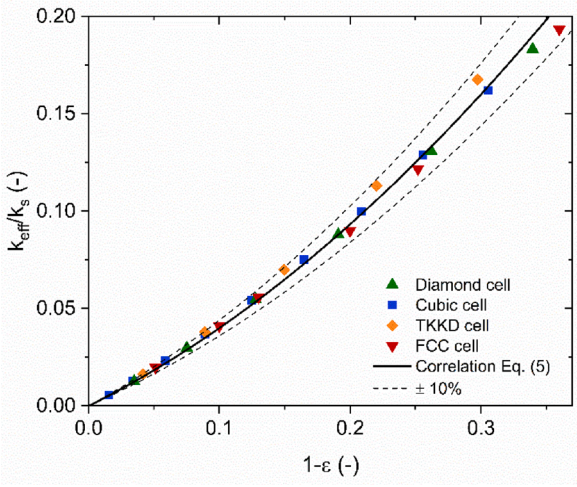

Fig. 5. Comparison between the dimensionless effective thermal conductivity of several POCS elementary cells (full symbols) and the correlation proposed by Bracconi et al. [20] (solid continuous line).

The performances of POCS have been also compared with those of open-cell foams. Fig. 3 shows that in the region of high void fractions, which is typical of metal foams, POCS overcome the open-cell foams performances by up to 15 %. On the other hand, the performances of foams and POCS are superimposed when the solid fraction (1-ε) is higher than 0.12.

Rather than to intrinsic differences between ordered and random structures, this is ascribed to the different distribution of the solid material along struts and in the nodes which characterizes POCS and open-cell foams. POCS, in fact, are characterized by a constant strut diameter which results in a uniform distribution of the solid material along the strut. Conversely, open-cell foams show a non-uniform diameter along the strut axis which increases moving from the middle section to the nodes (i.e. the regions where the struts join). These struts can be approximated by a parabolic trend along the strut axis as reported by Ambrosetti et al. [46]. The effect of the distribution of the solid material in open cellular structures has a significant impact on their effective thermal conductivity, as reported by Bracconi et al. [20] for open-cell foams and by Freund and coworkers [42] for POCS. These studies revealed that the uneven distribution of solid material along the struts reduces the effective heat transfer performances with respect of a corresponding structure with the same solid fraction but uniformly distributed. Bracconi et al. [20] also showed that ideal foams (e.g. manufactured via 3D printing) with a uniform strut profile exhibit improved effective conductivities, mostly in the region of low solid fractions. In this view, Fig. 4 compares the performances of both POCS and ideal open-cell foams with a uniform strut diameter (R = 1) [20], showing that the effective conductivity of ordered and random structures are indeed superimposed in the region of high void fraction.

The parabolic model of the strut profile shows that the ratio between the strut diameter at the nodes and at the middle of the struts decreases on increasing the solid content [20]. This is the reason for the fading difference between POCS and foams on decreasing the porosity. At high solid fractions, the decreasing effect of the strut profile is compensated by secondary effects of the topology of the nodes. It is worth noting that TKKD, whose topology more closely resembles the foam one [41], exhibit slightly superior effective conductivity performances in the entire investigated range of porosity.

3.5. Engineering correlation

We have derived an engineering correlation for the effective thermal conductivity of POCS as a function of the geometrical properties of the unit cell. According to our results, the only relevant dependence is the one on the solid fraction, which is derived in analogy with our previous work on open-cell foams [20]. The effective thermal conductivity is modeled according to Eq.(3), originally suggested by Freund and co-workers [42]:

$$\frac{k_{eff}}{k_s} = \frac{1-\varepsilon}{\tau} \tag{3}$$

where ε is the void fraction and τ is a tortuosity parameter. Recently, Bracconi et al. [20] proposed a correlation for the tortuosity of open-cell foams according to Eq. (4).

$$\tau = \frac{1}{(A(1-\varepsilon)+B)} \tag{4}$$

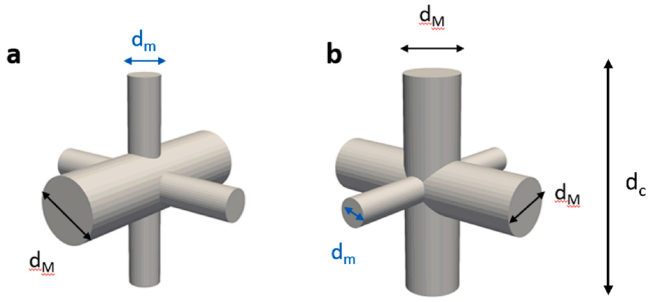

Fig. 6. Cubic cell with local anisotropy: mono-preferential (a) and bi-preferential (b) directions. The enlarged (d_M) and shrunk (d_m) strut sizes are highlighted along with cell dimension (d_c).

where A and B are constants evaluated from the asymptotic results of Maxwell [47] and Lemlich [48] valid for the porosity approaching zero and one, respectively. Lemlich [48] theoretically derived that the tortuosity of soap froth in the limit of porosity approaching one is equal to 3. On the other hand, the tortuosity of a full brick of solid material, corresponding to the limit of porosity approaching zero, is equal to one. By imposing the two asymptotes, it is possible to recover the value of $A = 2/3$ and $B = 1/3$ without any fitting of numerical or experimental data.

The effective thermal conductivity assumes therefore the expression of Eq. (5).

$$\frac{k_{eff}}{k_s} = \frac{1-\varepsilon}{\left(\frac{2}{3}(1-\varepsilon)+\frac{1}{3}\right)^{-1}} \tag{5}$$

Fig. 5 shows that Eq. (5) matches well the results of the numerical simulations carried out in this work. Thus, the correlation proposed by Bracconi et al. [20] for open-cell foams is able to accurately describe the effective thermal conductivity of POCS, too, without any additional adjustment of the parameters.

4. Cell anisotropy

The parametrical analysis carried out on POCS reveals that the effective thermal conductivity of the sole solid matrix is neither significantly affected by the cell shape nor by the direction of the cell in space. Hence, the cell topology does not provide additional degrees of freedom besides the solid fraction to tailor the heat transfer performances of the structure. In contrast, the distribution of the solid material along the struts has been observed to play a significant role in the definition of the structure performances [20,42]. By combining these results, we propose to modify the solid distribution within the cell by engineering the geometry of the struts in order to, consequently, tune its effective thermal conductivity.

Notably, the redistribution of the solid material in the cell at constant porosity determines the generation of anisotropic unit cells. Since the performances of the structure are independent of the cell shape, the analysis of the effect of the local anisotropy has been carried out for the cubic cell only. In fact, the simple geometry of this cell allows for a facile derivation of dedicated geometrical models useful for the generation of the virtual structure and for the analysis of the data.

The anisotropy is introduced in the structure by modifying the strut diameters along different directions. The expected effect is the tuning of the effective thermal conductivity in specific directions according to the specific process requirement. In this view, the generation of the structure is carried out by defining the amount of solid material loaded in the structure and, then, by evaluating the different distributions along the three spatial directions.

Fig. 6 shows two possible configurations of anisotropic cells characterized by the same amount of solid material (i.e. solid fraction), where the material is preferentially distributed along one or two directions. Fig. 6(a) represents a cubic POCS with an increment of the strut diameter in one direction, consequently the struts in the other two directions shrink to allow for conservation of the solid fraction. This structure, named cubic mono-preferential (C1P), is expected to promote the effective thermal conductivity in one direction, reducing, at the same time, the performances in the other two, resulting in an effective solution for the development of Lumped Thermal Reactors [43], where the main target is the promotion of axial thermal conductivity [49]. Conversely, Fig. 6(b) shows the other possible structure characterized by an enlargement of the strut diameter in two orthogonal directions, named cubic bi-preferential (C2P). This structure may be an interesting option when the promotion of radial thermal conductivity is the key target for energy intensive catalytic processes in tubular reactors.

4.1. Geometrical model

The geometry of the isotropic elementary cells is totally characterized once two out of three of the following quantities are defined: the cell size d_c, defined as the distance between the axes of two parallel struts, the porosity ε and the diameter of the struts d_s. Anisotropic structures are characterized by two different strut diameters d_M and d_m corresponding to the larger and smaller diameter, respectively. It is possible to introduce a parameter θ as the ratio of the diameter of the larger to the smaller strut, Eq. (6):

$$\theta = \frac{d_M}{d_m} \tag{6}$$

This parameter accounts for the distribution of the solid material in the structure and it can be regarded as an extent of anisotropy.

The four geometrical properties (i.e., cell size, porosity, maximum strut diameter and θ) are not independent. The definition of three of them is sufficient to totally characterize the geometry of the structures. In this work, we develop geometrical relationships which link the porosity, the cell size and the ratio between the strut diameters. For the generation of the structures, the diameter of the larger strut d_M is then calculated.

4.1.1. Mono-preferential (C1P) structures

The geometry of the cross element at each node of the cubic cell structure in Fig. 6(a) could be represented as a cylinder with d_M size with a length equal to cell size from which four smaller cylinders depart. The geometrical model is derived according to this description of the cells. As a result, the unit cell solid volume is equal to the sum of the volume of the large-diameter strut (V_M) along with the contribution of the small-diameter struts (V_m).

$$1-\varepsilon = \frac{V_M + 4\,V_m}{V_{cell}} \tag{7}$$

The volume of the strut with d_M diameter is computed according to Eq. (8),

$$V_M = \frac{\pi}{4} d_M^2 d_c \tag{8}$$

On the other hand, the volume of the struts characterized by d_m size can be evaluated as in Eq. (9). Additional details on the derivation are reported in Appendix A2.

$$V_m = \frac{\pi}{8}\frac{d_M^2}{\theta^2}\left(d_c - d_M\sqrt{1-\frac{1}{\theta^2}}\right) - \frac{d_M^3}{4\theta}\left(\arcsin\left(\frac{1}{\theta}\right) - \frac{1}{\theta}\sqrt{1-\frac{1}{\theta^2}}\right) \tag{9}$$

Finally, the solid fraction is evaluated according to Eq. (10)

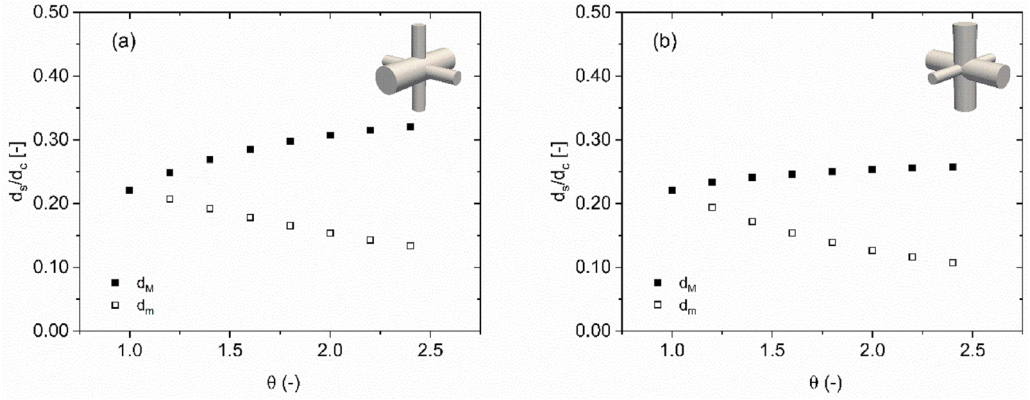

Fig. 7. Dimensionless strut diameters in enlarged (full square) and shrunk (empty square) for C1P (a) and C2P structures (b) for $\varepsilon = 0.9$.

$$(1-\varepsilon)_{C1P} = \frac{\frac{\pi}{4}d_M^2 d_c + \frac{\pi}{2}\frac{d_M^2}{\theta^2}\left(d_c - d_M\sqrt{1-\frac{1}{\theta^2}}\right) - \frac{d_M^3}{\theta}\left(\arcsin\left(\frac{1}{\theta}\right) - \frac{1}{\theta}\sqrt{1-\frac{1}{\theta^2}}\right)}{d_c^3} \tag{10}$$

4.1.2. Bi-preferential (C2P) structures

The geometrical model for the structure in Fig. 6(b) is developed based on the cubic cell model by Klumpp et al. [44]. The porosity of the structure is evaluated as the complement to one of the solid fraction of one cell. The unit cell consists of 8 nodes, positioned at the virtual vertices of the cube, and 12 struts, positioned at the edges of the cube. Within the structure, each strut and node are shared among 4 and 8 cells respectively. As a result, the unit cell solid volume is equal to the sum of the volume of one node and three struts:

$$1 - \varepsilon = \frac{V_{struts} + V_{node}}{V_{cell}} \tag{11}$$

where V_{cell} is the volume of the cubic cell, V_{struts} represents the volume occupied by the struts and V_{node} is the volume of the node.

The volume of the node is represented by the intersection of ligaments of different diameters. However, the mathematical modeling of such entity in the case of the anisotropic structures is complex and would involve the solution of non-analytical integrals. Hence, the volume of the node is calculated as reported by Klumpp et al. [44] for isotropic unit cells by considering the node with diameter d_M.

$$V_{node} = \left(\frac{3}{4}\pi - \sqrt{2}\right)d_M^3 \tag{12}$$

Since the node is assumed to be of d_M size, all the strut volumes are computed by considering a cylinder shortened by the node characteristic size.

The C2P elementary cell consists of two struts with diameter d_M and one with diameter d_m. Hence, the volume of the struts is evaluated according to Eq. (13):

$$V_{strut}^{C2P} = \frac{\pi}{4}\left(\frac{d_M}{\theta}\right)^2(d_c - d_M) + \frac{\pi}{2}d_M^2(dc - d_M) \tag{13}$$

Finally, the solid fraction is evaluated according to Eq. (14):

$$(1-\varepsilon)_{C2P} = \frac{\left(\frac{\pi}{4\theta^2} + \frac{\pi}{2}\right)(d_c - d_M)d_M^2 + \left(\frac{3}{4}\pi - \sqrt{2}\right)d_M^3}{d_c^3} \tag{14}$$

4.1.3. Geometrical model results

Eq. (10) and Eq. (14) are cubic equations in the large strut diameter, d_M. The equations have three real solutions: one of them is negative, one is larger than the cell size, and the physically meaningful one is comprised between zero and the cell size. The value of d_m can be easily recovered once the solution of d_M is found for the assigned values of d_c, ε and θ. In this view, θ up to 2.4 have been considered since larger values might lead to structures with very thin ligaments or with a slenderness (i.e. ratio between the strut length and diameter) which prevents the manufacturing via 3D printing.

Several CADs of the structures with various porosity, cell diameter and ratio θ have been generated to assess the accuracy of the geometrical models. The solid fraction evaluated on the CAD has been compared with the one predicted by the geometrical model, and an excellent agreement has been observed with a relative variation at most of 2% for the mono-modified structure at porosity 0.7.

Fig. 7 shows the trends of d_M and d_m normalized by the cell diameter for the two anisotropic structures as a function of θ for $\varepsilon = 0.9$. The C1P

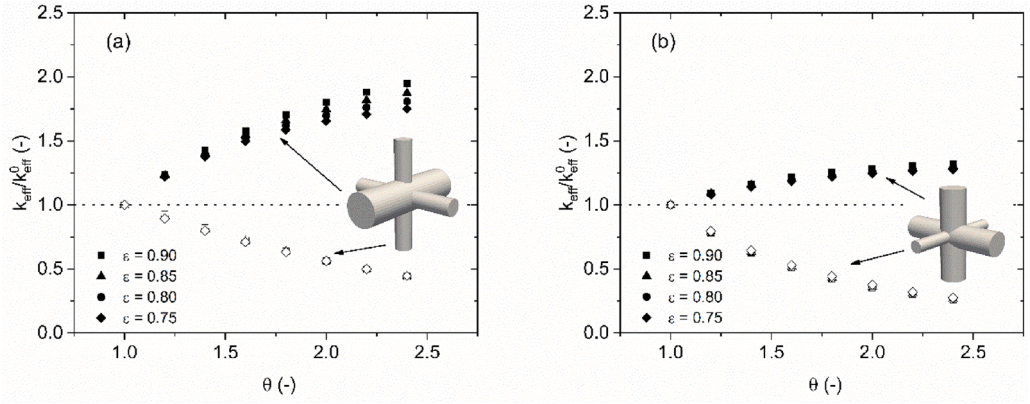

Fig. 8. Effective thermal conductivity of C1P (a) and C2P (b) anisotropy structures normalized by the isotropic one as a function of the anisotropy factor θ.

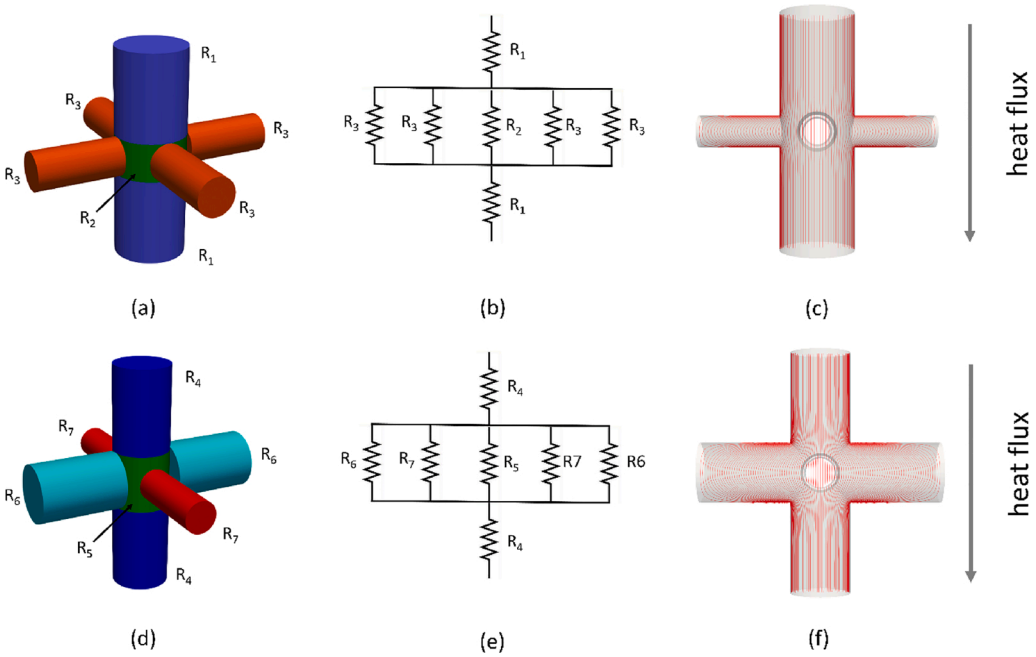

Fig. 9. Simplified model of the unit cell of a C1P structure (a) along the equivalent electrical network (b) and heat flow lines in the structure (c); simplified model of the unit cell of a C2P structure (d) along the equivalent electrical network (e) and heat flow lines in the structure (f).

cell shows an almost symmetrical behavior with an increment of d_M in one direction up to 40 % and a corresponding 40 % reduction of d_m in the other two directions for a value of $\theta = 2.4$. On the other hand, the C2P cell shows an asymmetrical behavior with a lower increment (i.e., 16 % for $\theta = 2.4$) of the strut size for the large ligaments compensated by a larger reduction of the strut size for the smaller ligament (i.e., 51 % for $\theta = 2.4$) to guarantee a constant solid volumetric fraction.

4.2. *Effective thermal conductivity of anisotropic structures*

The effective thermal conductivity of the anisotropic structures has been investigated by parametrically changing both θ and the porosity. A porosity range between 0.75 and 0.9 has been explored covering a broad interval of possible geometries. All the structures have been generated with a cell size equal to 3 mm since the results are independent of the cell size.

Fig. 8(a) shows the effective thermal conductivity as a function of θ for C1P structures normalized to the effective thermal conductivity of the isotropic structure with the same porosity. First, the presence of the preferential solid distribution is clearly able to differentiate the performances and to selectively increase or decrease the thermal conductivity in a specific direction. By considering the direction in which the struts are enlarged, the effective thermal conductivity increases with θ for every void fraction. For instance, in the case of a 0.9 porosity the different distribution of the solid material provides an effective heat conductivity up to twice the value of the isotropic structure. This is ascribed to the larger strut diameter in that direction which provides a higher cross-sectional area and consequently lower resistance to the conductive heat transfer. It is worth noticing that the porosity influences the relative increment in the thermal conductivity. In particular, the lower is the porosity the smaller is the relative gain in terms of effective thermal conductivity. This is due to the different contributions of struts and nodes to the overall solid distribution. The relative amount of the solid volume allocated in the nodes decreases with the porosity, moving from 40 % at 0.75 to 20% at 0.9. In this view, the solid available for the redistribution, which is mainly located in the struts, increases with growing porosity. Hence, the effect of redistribution of the solid material due to the anisotropy is stronger at high porosity.

It is possible to predict the asymptotic behavior of the structures at large values of θ ($\theta \rightarrow \infty$), which represents the maximum possible performance improvement. Such evaluation is quite simple in the case of C1P structures since they would collapse in an ensemble of parallel cylinders in the direction of the increased strut diameter with no connections in the other directions. The schematic representation of the unit cell becomes a single cylinder with a diameter equal to d_M. Hence, the effective thermal conductivity can be estimated simply as:

$$\frac{k_{eff}}{k_s} = 1 - \varepsilon \tag{15}$$

Eq (15) is notably the same equation of the effective axial thermal conductivity of honeycomb monoliths [50].

By employing Eq. (5) for the description of the isotropic structure the asymptotic relative increase of the effective thermal conductivity in the preferential direction becomes as in Eq. (16):

$$\frac{k_{eff}}{k^0_{eff}} = \frac{1}{\frac{2}{3}(1-\varepsilon)+\frac{1}{3}} \tag{16}$$

Eq. (16) reveals that the asymptotic value is a function of the porosity of the structure: the higher is the porosity the larger is the asymptotic value and the potential gain of the anisotropic structure. For example, the asymptotic performance gain observed in two structures with a porosity of 0.9 and 0.7 are 2.5 and 2.0, respectively.

The effective thermal conductivity in the direction where the struts are thinner decreases with θ. This is ascribed to the lower strut diameter in this direction and, consequently, to the higher heat transfer resistance. A reduction of the thermal conductivity up to 2 times is observed with respect to the isotropic case. In this direction, the effect of the porosity is negligible since the profiles for the different porosities are superimposed. This is explained by the fact that the limiting heat transfer resistance is due to the cross section of the struts rather than to the cross section of the node, therefore, a negligible influence of the porosity is observed.

Fig. 8(b) shows the effective thermal conductivity of C2P structures normalized by the effective thermal conductivity of the isotropic structure with the same porosity as a function of θ.

Similarly to C1P structures, it is possible to increase the perfor-

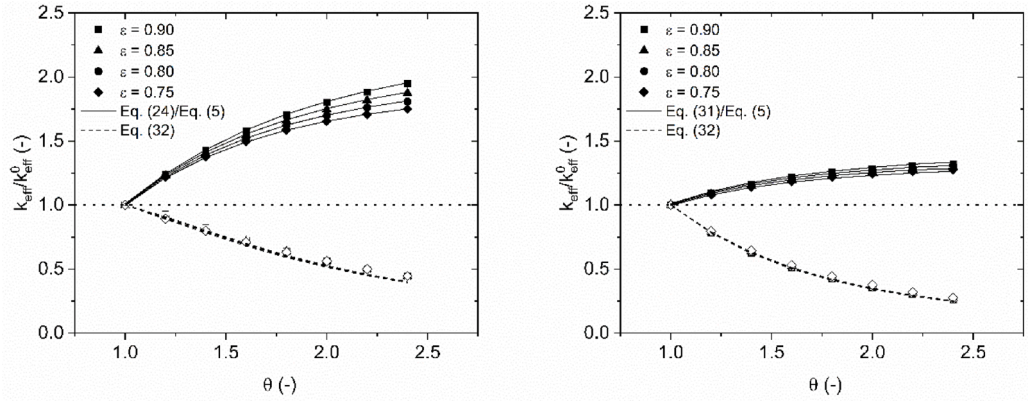

Fig. 10. Effective thermal conductivity of C1P (a) and C2P (b) anisotropy structures evaluated based on the heat conductivity models normalized by the isotropic one as a function of the anisotropy factor θ.

mances in the two directions characterized by the larger ligaments by increasing θ. In particular, the effective thermal conductivity in the privileged directions can be increased up to 40 % with respect to the isotropic structures. It can be noticed that the improvement is lower than in the previous case. This is due to fact that the increment of the cross-sectional area of the struts is distributed onto two ligaments resulting in a lower gain. On the other hand, a decrement of the performances in the remaining direction is still present. Moreover, the porosity is observed to have an impact on the performances in the directions of larger strut diameters while a minor effect is observed in the other direction. The reason of this behavior is ascribed once again to the non-linear effect of the nodes in the distribution of the solid material, resulting in different effects over the directions.

4.3. Engineering correlation

In this section, we propose engineering correlations aiming at the prediction of the effective thermal conductivity of anisotropic structures based on their geometrical parameters.

First, the derivation of the model in the case of C1P structures is presented. We consider the anisotropic cubic cell POCS shown in Fig. 9 (a) and we derive a model for the k_{eff} by means of an approximate analysis of the thermal conductivity in the unit cell according to an electrical network analogy. In case of a uniform temperature difference along the vertical direction, heat flows through the unit cell by conduction in the solid matrix. We decompose the unit cell into a set of cylindrical elements characterized by three specific thermal resistances as shown in Fig. 9. In this view, the cell resistance and therefore the effective thermal conductivity ($k_{eff} = \frac{1}{R_c}\frac{L_{cell}}{A_{cell}}$) is computed through an electrical analogy by means of a combination of resistances in series and in parallel, as shown in Fig. 9(b).

The resistance to heat transfer R_1 is evaluated as follows:

$$R_1 = \frac{1}{k_s}\frac{0.5\,(d_c - d_m)}{\frac{\pi}{4}d_M^2} \tag{17}$$

The heat resistance of the portion of structure generated by the node and the lateral branches requires to account for the progressive variation of the cross-section on the lateral struts which depends on the position along the vertical direction in Fig. 9(a). In this view, the equivalent resistance for this portion is equal to the series of an infinite number of parallel entities generated by the core cylinder (R_2) and the lateral struts (R_3)

In particular, the differential resistance to heat transfer dR_2/dz of the core of the node is evaluated as follows:

$$\frac{dR_2}{dz} = \frac{1}{k_s}\frac{4}{\pi d_M^2} \tag{18}$$

The differential resistance of the lateral branches can be calculated with similar equations. However, one additional parameter is required to consider the elongation of heat flux lines present when moving from the straight central strut to the lateral branches. For this reason, we consider ψ as a solid tortuosity of the lateral branches to properly account for their effective length. The heat flux lines in the solid structure, which are straight and parallel until they reach the node, slightly deviate due to the presence of the lateral branches (Fig. 9(c)), implying an additional resistance.

$$\frac{dR_3}{dz} = \frac{1}{k_s}\frac{\psi}{(d_c - d_M)\sqrt{\frac{d_m^2}{4} - z^2}} \tag{19}$$

The tortuosity factor ψ accounts for two effects. On one side, the longer path that the heat flow lines have to travel in the region of the intersection between the nodes and the lateral branches. Analytically, we can compute the maximum length of a heat flux line for our geometry as reported in Eq. (20). It is evident that the heat flow lines can be extended at most by a quantity equal to a lateral strut length. On the other hand, the region of change in the cross-section introduces additional and localized heat transfer resistances which are hard to be analytically quantified. The thermal conductivity model herein developed for anisotropic POCS structures was applied to isotropic structures, where numerical correlations have been previously described. In this case a correction factor equal to 2 was necessary to reconciliate the results of the model and the previous simulations. We observed that a tortuosity factor as reported in Eq. (20) can accurately describe such phenomena in the range of solid fraction of interest (i.e., $1 - \varepsilon < 0.4$) also for anisotropic structures.

Hence:

$$\psi = 2\frac{d_c + d_m - d_M}{d_m} \tag{20}$$

The equivalent resistance of the node-strut intersection is as reported in Eq. (21).

$$\begin{aligned} R_{eq} &= \int_{-\frac{d_m}{2}}^{\frac{d_m}{2}} \left(\frac{4dz}{dR_2} + \frac{dz}{dR_3}\right)^{-1} dz = \frac{1}{k_s}\int_{-\frac{d_m}{2}}^{\frac{d_m}{2}} \frac{dz}{\frac{\pi}{4}d_M^2 + \frac{4}{\psi}(d_c - d_M)\sqrt{\frac{d_m^2}{4} - z^2}} \\ &= \frac{1}{k_s}\int_{-r}^{r} \frac{dz}{a + b\sqrt{r^2 - z^2}} \end{aligned} \tag{21}$$

where $a = \frac{\pi}{4}d_M^2$, $b = \frac{4}{\psi}(d_c - d_M)$ and $r = \frac{d_m}{2}$.

The integral has an analytical solution which is reported in Eq. (22):

$$R_{eq}^{mono} = \frac{1}{k_s}\left(\frac{a}{b\sqrt{a^2 - b^2r^2}}\left(2\arctan\left(\frac{br}{\sqrt{a^2 - b^2r^2}}\right) - \pi\right) + \frac{\pi}{b}\right) \tag{22}$$

The cell resistance becomes:

$$R_c^{mono} = 2\,R_1 + R_{eq}^{mono} \tag{23}$$

Finally, the normalized effective thermal conductivity reads as Eq (24):

$$\frac{k_{eff}}{k_s} = \frac{1}{d_c R_c^{mono}} = \frac{1}{d_c} \frac{1}{\left(\frac{(d_c-d_m)}{\frac{\pi}{4}d_M^2} + \frac{a}{b\sqrt{a^2-b^2r^2}}\left(2\arctan\left(\frac{br}{\sqrt{a^2-b^2r^2}}\right)-\pi\right)+\frac{\pi}{b}\right)} \tag{24}$$

In Fig. 10(a), the normalized effective thermal conductivity predicted by the model is plotted against the value obtained by the numerical simulations. An excellent agreement is observed with deviations at most of the 3% at low θ and high porosity. Moreover, it is possible to demonstrate that the model correctly predicts both the asymptotic behaviors at $\theta \to 1$ and $\theta \to \infty$.

The effective thermal conductivity of the C2P structure is evaluated along the same lines. Once again, the structure is sketched as resistances in series and in parallel, as shown in Fig. 9(d). In particular, three resistances in series are considered. In total analogy with C1P, the first resistance is that of the strut with d_M size followed by the resistance of the node and, finally, by a resistance of the strut with d_M size, as shown in Fig. 9(e).

The resistance to heat transfer R_4 is evaluated as follows:

$$R_4 = \frac{1}{k_s}\frac{0.5\,(d_c - d_M)}{\frac{\pi}{4}d_M^2} \tag{25}$$

The heat resistance of the portion of structure generated by the node and the lateral branches requires to account for the progressive variation of the cross-section on the lateral struts which depends on the position along the vertical direction keeping in mind also the presence of struts with different diameters.

The resistance to heat transfer dR_5/dz of the core of node is evaluated as follows:

$$\frac{dR_5}{dz} = \frac{1}{k_s}\frac{4}{\pi d_M^2} \tag{26}$$

The differential resistance of the lateral branches can be calculated with similar equations but requires once again a tortuosity factor. The different size and structures of the lateral branches requires to introduce a different factor for each to account for the enlengthened flow lines and additional thermal resistance in the node. These two coefficients are calculated in analogy with the C1P structure.

$$\frac{dR_6}{dz} = \frac{1}{k_s}\frac{\psi_I}{(d_c - d_M)\sqrt{\frac{d_M^2}{4} - z^2}} \tag{27}$$

$$\frac{dR_7}{dz} = \frac{1}{k_s}\frac{\psi_{II}}{(d_c - d_M)\sqrt{\frac{d_m^2}{4} - z^2}} \tag{28}$$

where $\psi_I = 2\frac{d_c}{d_M}$ and $\psi_{II} = 2\frac{d_c + d_m - d_M}{d_m}$

The equivalent resistance for this portion is equal to the series of an infinite number of parallel entities generated by the core cylinder (R_5) and the lateral struts (R_6 and R_7).

$$R_{eq}^{bi} = \int_{-\frac{d_M}{2}}^{-\frac{d_m}{2}} \left(\frac{dz}{dR_5} + \frac{2dz}{dR_6}\right)^{-1} dz + \int_{-\frac{d_m}{2}}^{\frac{d_m}{2}} \left(\frac{dz}{dR_5} + \frac{2dz}{dR_6} + \frac{2dz}{dR_7}\right)^{-1} dz + \int_{\frac{d_m}{2}}^{\frac{d_M}{2}} \left(\frac{dz}{dR_5} + \frac{2dz}{dR_6}\right)^{-1} dz \tag{29}$$

By combining Eq (25)–(29), we obtain

$$R_c^{bi} = 2\,R_4 + R_{eq}^{bi} = \frac{1}{k_s}\frac{(d_c - d_M)}{\frac{\pi}{4}d_M^2} + \int_{-\frac{d_M}{2}}^{-\frac{d_m}{2}} \left(\frac{dz}{dR_5} + \frac{2dz}{dR_6}\right)^{-1} dz + \int_{-\frac{d_m}{2}}^{\frac{d_m}{2}} \left(\frac{dz}{dR_5} + \frac{2dz}{dR_6} + \frac{2dz}{dR_7}\right)^{-1} dz + \int_{\frac{d_m}{2}}^{\frac{d_M}{2}} \left(\frac{dz}{dR_5} + \frac{2dz}{dR_6}\right)^{-1} dz \tag{30}$$

The expression of Eq. (30) is not analytically determinable, therefore it should be integrated numerically.

Finally, the normalized effective thermal conductivity reads as Eq (31):

$$\frac{k_{eff}}{k_s} = \frac{1}{d_c R_c^{bi}} \tag{31}$$

The model is in excellent agreement with the results of the simulations with minor deviations (< 3%) at low θ, as shown in Fig. 10(b).

Finally, the thermal conductivity in the direction characterized by the reduced strut diameter can be modeled by considering the heat transfer resistances of the strut with reduced sections for both the anisotropic structures. All the heat transfer resistances are located in the strut with small diameter while the effect of the resistance in the nodes can be considered negligible. Hence, the ratio between the effective thermal conductivity of the anisotropic and the isotropic structures is proportional to the ratio of the thermal resistances of the struts as reported in Eq. (32)

$$\frac{k_{eff}}{k_{eff,0}} = \frac{\frac{\pi}{4}(d_c - d_s)d_m^2}{\frac{\pi}{4}(d_c - d_M)d_s^2} \tag{32}$$

A good agreement is obtained with the numerical simulations as illustrated in Fig. 10.

5. Conclusions

In this work, we have extensively analyzed the effective solid thermal conductivity of isotropic and anisotropic periodic open cellular structures by means of 3D simulations on virtually generated samples. In case of isotropic structures, our analysis revealed that, among the main geometrical properties of the structures, the only relevant parameter for the determination of the thermal conductivity is the porosity, whereas other features such as the cell size and shape do not significantly affect this parameter. Accordingly, it is possible to correlate the effective thermal conductivities of different cell shapes using a single correlation that matches the physical behaviors at the boundaries of the porosity range. Finally, these structures offer an advantage with respect to open-cell foams, thanks to their optimal solid distribution inside uniform ligaments.

In this work, we have also proposed two anisotropic structures, based on the cubic unit cell, where the ligaments in two or one direction are thicker. With the envisioned solution, at fixed porosity of the material, it is possible to increase the thermal conductivity by up to 100 % or 40 % with respect to the conventional structure in the axial or in the radial direction, respectively. Thanks to the thinner strut in the opposite direction, the thermal conductivity in the other direction is reduced by a factor up to 5, which is a particularly relevant result for insulation applications. Finally, mathematical correlations based on the geometrical features of the structures were derived for the quantification of the effective thermal conductivities of the anisotropic structures.

As a whole, we have fully characterized the effective thermal conductivity of a solid matrix for a wide set of geometries and configurations. These solutions are extremely promising for the intensification of many energy-intensive processes and, specifically, they can provide additional degrees of freedom when it is required to boost the heat

transfer either in the radial direction (e.g. in the case of multi-tubular reactors with heat exchange) or in the axial direction (e.g. in adiabatic and lumped thermal reactors). In view of the design of such reactors, additional investigations (e.g. on pressure drop, convective heat transfer) will be required towards the optimal design of the next generation of process technology.

CRediT authorship contribution statement

Mauro Bracconi: Data curation, Methodology, Investigation, Software, Validation, Formal analysis, Visualization, Conceptualization, Writing - original draft. **Matteo Ambrosetti:** Investigation, Validation, Formal analysis, Visualization, Conceptualization, Writing - original draft. **Matteo Maestri:** Conceptualization, Methodology, Resources, Writing - review & editing, Supervision. **Gianpiero Groppi:** Conceptualization, Methodology, Resources, Writing - review & editing, Supervision. **Enrico Tronconi:** Conceptualization, Resources, Writing - review & editing, Supervision, Project administration, Funding acquisition.

Declaration of Competing Interest

The authors report no declarations of interest.

Acknowledgements

This project has received funding from the European Research Council under Grant Agreement no. 694910 (INTENT). Computational time at CINECA (Bologna) is gratefully acknowledged.

Appendix A. Geometrical model for face-centered-cubic (FCC) cells

The FCC unit cell is constituted by 8 nodes, positioned at the virtual vertices of the cube, along with 18 struts, 12 positioned at the edges of the cube and 6 crossing the faces according to Fig. 1. Within the structure, each node is shared among 8 cells. Moreover, each edge strut is shared among 4 cells while the face-transversal struts are shared between two faces.

As a result, the unit cell solid volume is equal to the sum of the volume of one node, three edges and three face-transversal struts.

$$1-\varepsilon=\frac{3\ V_{struts}^{edges}+3\ V_{struts}^{faces}+V_{node}}{V_{cell}} \tag{A1}$$

The volume of the node is represented by the intersection of ligaments. The number of ligaments which converges in each node can be either 6 as in conventional cubic cells or 9 according to the position. The mathematical modeling of such entity in the case of conventional cubic cell can be analytically modeled by the Steinmetz solid [44]. However, the description in case of FCC is much more complex and would involve the solution of non-analytical integrals. Hence, the volume of the node is assumed to be the same employed in the regular cubic cell, i.e. by considering the intersection of three struts.

$$V_{node}=\left(\frac{3}{4}\pi-\sqrt{2}\right)d_s^3 \tag{A2}$$

The volume of the edge struts is computed as in the case of conventional cubic cell as a cylinder characterized by a length equal to the cell size reduced by the node diameter (d_s) [44]

$$V_{strut}^{edges}=\frac{\pi}{4}d_s^2(d_c-d_s) \tag{A3}$$

The volume of the face struts is approximated as a cylinder with a diameter equal to d_s and a length equal to the diagonal of the face shortened by the region of intersection between faces struts with edges and nodes as shown in Fig. A1

Hence, the volume of the strut is computed according to Eq. (A4)

$$V_{strut}^{edges}=\frac{\pi}{4}d_s^2\left(\sqrt{2}\,d_c-\left(\sqrt{2}+1\right)d_s\right) \tag{A4}$$

As a result, the solid fraction is computes as follows.

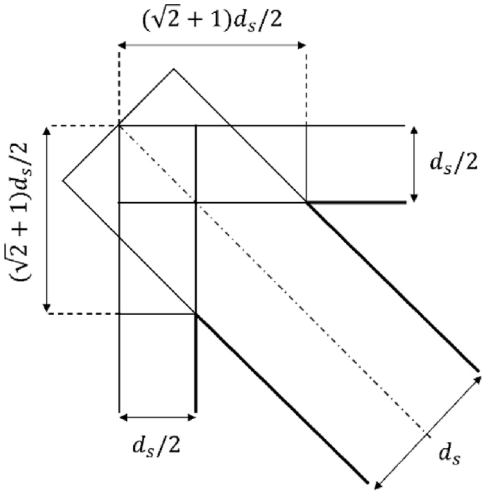

Fig. A1. Detail of the strut intersection in node for an FCC cell.

$$1-\varepsilon=\frac{\left(\frac{3}{4}\pi-\sqrt{2}\right)d_s^3+\frac{3}{4}\left(\left(\sqrt{2}+1\right)d_c-\left(\sqrt{2}+2\right)d_s\right)d_s^2\pi}{d_c^3} \tag{A5}$$

Appendix B. Geometrical model for strut volume with d_m size in configuration mono-modified

The geometrical model for the anisotropy unit cell with the increment in a single direction requires to compute the volume of the struts with d_m diameter. The strut is modeled as a cylinder intersecting the strut in the other directions, as shown in Fig. A2.

The volume V_m of the strut is computed as the difference between the volume of a cylinder of length l and diameter d_m and the volume of the red region in Fig. A2 which represents the intersection between the two cylinders. The length l of the cylinder is evaluated by considering the semilength of a strut reduced by the distance h_a (see Fig. A3).

$$l=\frac{d_c}{2}-h_a=\frac{d_c}{2}-\sqrt{r_M^2-r_m^2} \tag{A6}$$

The volume of the intersection V_{int} (red region in Fig. A2) is computed by integrating the area of the intersection between $-r_m$ and r_m.

$$V_{int}=\int_{-r_m}^{r_m}A(z)dz \tag{A7}$$

The area is function of the position along the large strut axis as shown in Fig. A3. By considering a general position z, the area can be computed as the sum of a rectangular region A_r (blu area in Fig. A3) plus the circular segment A_s (green area in Fig. A3).

$$A(z)=A_r(z)+A_s(z) \tag{A8}$$

The area of the rectangle is computed as reported in Eq. A9

$$A_r(z)=2\,h_r\;\;t=2\left(\sqrt{r_M^2-t^2}-\sqrt{r_M^2-r_m^2}\right)\;\sqrt{r_m^2-z^2}=2\left(\sqrt{r_M^2-r_m^2+z^2}-\sqrt{r_M^2-r_m^2}\right)\;\sqrt{r_m^2-z^2} \tag{A9}$$

The area of the circular segment is equal to the difference of the area of the circular sector characterized by a central angle of 2φ and the area of the triangle.

$$A_s(z)=\varphi r_M^2-(h_a+h_r)\;\;t=\varphi r_M^2-\sqrt{r_M^2-r_m^2+z^2}\;\;\sqrt{r_m^2-z^2} \tag{A10}$$

where $\varphi=\arcsin\left(\frac{\sqrt{r_m^2-z^2}}{r_M}\right)$

Hence, the volume of the strut reads as follows:

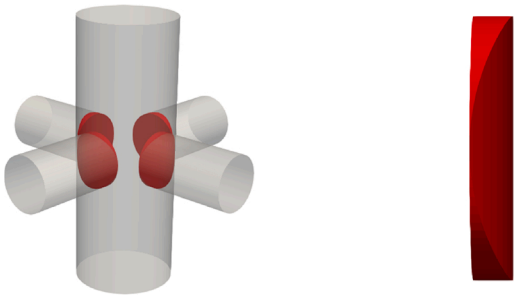

Fig. A2. Intersection between struts for the mono-modified anisotropic cell with the intersection region highlighted.

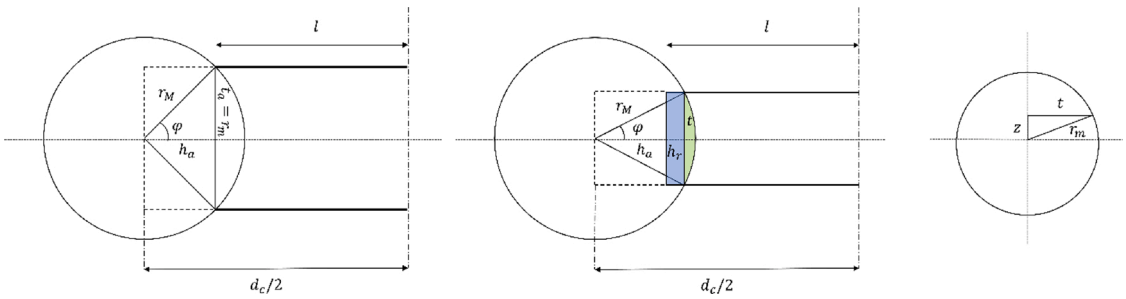

Fig. A3. Geometry of the intersection between struts for the mono-modified structures.

$$V_m = \frac{\pi}{4} d_m^2 \quad l - \int_{-r_m}^{r_m} A(z)dz \tag{A11}$$

The integral in Eq. A11 does not have an analytical solution hampering this approach. To overcome such a limitation, a simplified model of the intersection is proposed. The volume of the intersection is approximated to be equal to the volume of a prism with the circular segment evaluated at z = 0 as base and height the strut diameter d_m as height.

$$V_{int} = \int_{-r_m}^{r_m} A(z)dz \approx \left(\arcsin\left(\frac{r_m}{r_M}\right) r_M^2 - \sqrt{r_M^2 - r_m^2} \quad r_m \right) \quad d_m \tag{A12}$$

The simplified model evaluates a volume of the intersection which is around 13 % more than the value obtained by the rigorous model. Despite such difference, the volume of the four intersections in the node accounts for the 0.2 % of the total node volume. Thus, the overall error introduced by the simplified model in the evaluation of the strut volume and of the solid fraction is negligible.

As a whole, V_m is computed as follows

$$V_m = \frac{\pi}{4} d_m^2 \quad \left(\frac{d_c}{2} - \sqrt{r_M^2 - r_m^2} \right) - \left(\arcsin\left(\frac{r_m}{r_M}\right) r_M^2 - \sqrt{r_M^2 - r_m^2} \quad r_m \right) \quad d_m \tag{A13}$$

Appendix C. Supplementary data

Supplementary material related to this article can be found, in the online version, at doi:https://doi.org/10.1016/j.cep.2020.108169.

References

[1] E. Tronconi, G. Groppi, C.G. Visconti, Structured catalysts for non-adiabatic applications, Curr. Opin. Chem. Eng. 5 (2014) 55–67, https://doi.org/10.1016/j.coche.2014.04.003.

[2] A.I. Stankiewicz, J.A. Moulijn, Process intensification: transforming chemical engineering, Chem. Eng. Prog. 96 (2000) 22–34.

[3] G. Groppi, E. Tronconi, C. Cortelli, R. Leanza, Conductive monolithic catalysts: development and industrial pilot tests for the oxidation of o-xylene to phthalic anhydride, Ind. Eng. Chem. Res. 51 (2012) 7590–7596, https://doi.org/10.1021/ie2021653.

[4] E. Lahtinen, L. Turunen, M.M. Hänninen, K. Kolari, H.M. Tuononen, M. Haukka, Fabrication of porous hydrogenation catalysts by a selective laser sintering 3D printing technique, ACS Omega 4 (2019) 12012–12017, https://doi.org/10.1021/acsomega.9b00711.

[5] J. Xu, G.F. Froment, Methane steam reforming, methanation and water-gas shift: I. Intrinsic kinetics, AIChE J. 35 (1989) 88–96, https://doi.org/10.1002/aic.690350109.

[6] A. Egana, O. Sanz, D. Merino, X. Moriones, M. Montes, Fischer-tropsch synthesis intensification in foam structures, Ind. Eng. Chem. Res. 57 (2018) 10187–10197, https://doi.org/10.1021/acs.iecr.8b01492.

[7] A.G. Dixon, B. Partopour, Computational fluid dynamics for fixed bed reactor design, Annu. Rev. Chem. Biomol. Eng. 11 (2020) 109–130, https://doi.org/10.1146/annurev-chembioeng-092319-075328.

[8] G.D. Wehinger, Radiation matters in fixed-bed CFD simulations, Chemie-Ingenieur-Technik 91 (2019) 583–591, https://doi.org/10.1002/cite.201800179.

[9] G. Belussi, M. Bohnet, J. Bus, K. Drautz, H. Greim, K.-P. Jackel, U. Karts, A. Kleeman, G. Kreysa, T. Laird, W. Meier, E. Ottow, M. Roper, J. Scholtz, K. Sundmaker, R. Ulber, U. Wietelmann, Ullmann's Encyclopedia of Industrial Chemistry, 40 Volume Set, 7th edition, 2011.

[10] S.T. Sie, H.P. Calis, Structured Catalysts and Reactors, CRC Press, 2005, https://doi.org/10.1201/9781420028003.

[11] M. Sheng, H. Yang, D.R. Cahela, B.J. Tatarchuk, Novel catalyst structures with enhanced heat transfer characteristics, J. Catal. 281 (2011) 254–262, https://doi.org/10.1016/j.jcat.2011.05.006.

[12] K. Pangarkar, T.J. Schildhauer, J.R. van Ommen, J. Nijenhuis, J.A. Moulijn, F. Kapteijn, Experimental and numerical comparison of structured packings with a randomly packed bed reactor for Fischer-Tropsch synthesis, Catal. Today 147 (2009) 2–9, https://doi.org/10.1016/j.cattod.2009.07.035.

[13] S. Rebughini, M. Bracconi, A.G. Dixon, M. Maestri, A hierarchical approach to chemical reactor engineering: an application to micro packed bed reactors, React. Chem. Eng. 3 (2018) 25–33, https://doi.org/10.1039/c7re00195a.

[14] E. Bianchi, T. Heidig, C.G. Visconti, G. Groppi, H. Freund, E. Tronconi, Heat transfer properties of metal foam supports for structured catalysts: wall heat transfer coefficient, Catal. Today 216 (2013) 121–134, https://doi.org/10.1016/j.cattod.2013.06.019.

[15] M. Hettel, E. Daymo, O. Deutschmann, 3D modeling of a CPOX-reformer including detailed chemistry and radiation effects with DUO, Comput. Chem. Eng. 109 (2018) 166–178, https://doi.org/10.1016/j.compchemeng.2017.11.005.

[16] C. Sinn, F. Kranz, J. Wentrup, J. Thöming, G.D. Wehinger, G.R. Pesch, CFD simulations of radiative heat transport in open-cell foam catalytic reactors, Catalysts 10 (2020) 1–19, https://doi.org/10.3390/CATAL10060716.

[17] E. Tronconi, G. Groppi, T. Boger, A. Heibel, Monolithic catalysts with "high conductivity" honeycomb supports for gas/solid exothermic reactions: characterization of the heat-transfer properties, Chem. Eng. Sci. 59 (2004) 4941–4949, https://doi.org/10.1016/j.ces.2004.07.018.

[18] R. Balzarotti, M. Ambrosetti, A. Beretta, G. Groppi, E. Tronconi, Investigation of packed conductive foams as a novel reactor configuration for methane steam reforming, Chem. Eng. J. (2019) 123494, https://doi.org/10.1016/j.cej.2019.123494.

[19] P. Aghaei, C.G. Visconti, G. Groppi, E. Tronconi, Development of a heat transport model for open-cell metal foams with high cell densities, Chem. Eng. J. 321 (2017) 432–446, https://doi.org/10.1016/J.CEJ.2017.03.112.

[20] M. Bracconi, M. Ambrosetti, M. Maestri, G. Groppi, E. Tronconi, A fundamental analysis of the influence of the geometrical properties on the effective thermal conductivity of open-cell foams, Chem. Eng. Process. - Process Intensif. 129 (2018) 181–189, https://doi.org/10.1016/j.cep.2018.04.018.

[21] M. Ambrosetti, R. Balzarotti, C. Cristiani, G. Groppi, E. Tronconi, The influence of the washcoat deposition process on high pore density open cell foams activation for CO catalytic combustion, Catalysts 8 (2018) 510, https://doi.org/10.3390/catal8110510.

[22] C.G. Visconti, G. Groppi, E. Tronconi, Highly conductive "packed foams": a new concept for the intensification of strongly endo- and exo-thermic catalytic processes in compact tubular reactors, Catal. Today 273 (2016) 178–186, https://doi.org/10.1016/j.cattod.2016.02.060.

[23] M. Ambrosetti, M. Bracconi, M. Maestri, G. Groppi, E. Tronconi, Packed foams for the intensification of catalytic processes: assessment of packing efficiency and pressure drop using a combined experimental and numerical approach, Chem. Eng. J. 382 (2020) 122801, https://doi.org/10.1016/j.cej.2019.122801.

[24] R. Balzarotti, A. Beretta, G. Groppi, E. Tronconi, A comparison between washcoated and packed copper foams for the intensification of methane steam reforming, React. Chem. Eng 3 (2019) 1387–1392, https://doi.org/10.1039/C9RE00125E.

[25] L. Fratalocchi, C.G. Visconti, G. Groppi, L. Lietti, E. Tronconi, Intensifying heat transfer in Fischer-Tropsch tubular reactors through the adoption of conductive packed foams, Chem. Eng. J. 349 (2018) 829–837.

[26] A. Inayat, M. Klumpp, M. Lämmermann, H. Freund, W. Schwieger, Development of a new pressure drop correlation for open-cell foams based completely on theoretical grounds: taking into account strut shape and geometric tortuosity, Chem. Eng. J. 287 (2016) 704–719, https://doi.org/10.1016/j.cej.2015.11.050.

[27] C. Busse, H. Freund, W. Schwieger, Intensification of heat transfer in catalytic reactors by additively manufactured periodic open cellular structures (POCS), Chem. Eng. Process. Process Intensif. 124 (2018) 199–214, https://doi.org/10.1016/j.cep.2018.01.023.

[28] M. Lämmermann, G. Horak, W. Schwieger, H. Freund, Periodic open cellular structures (POCS) for intensification of multiphase reactors: liquid holdup and two-phase pressure drop, Chem. Eng. Process. - Process Intensif. 126 (2018) 178–189, https://doi.org/10.1016/j.cep.2018.02.027.

[29] E. Hansjosten, A. Wenka, A. Hensel, W. Benzinger, M. Klumpp, R. Dittmeyer, Custom-designed 3D-printed metallic fluid guiding elements for enhanced heat transfer at low pressure drop, Chem. Eng. Process. - Process Intensif. 130 (2018) 119–126, https://doi.org/10.1016/j.cep.2018.05.022.

[30] M. Bracconi, M. Ambrosetti, O. Okafor, V. Sans, X. Zhang, X. Ou, C.P. Da Fonte, X. Fan, M. Maestri, G. Groppi, E. Tronconi, Investigation of pressure drop in 3D replicated open-cell foams: coupling CFD with experimental data on additively

manufactured foams, Chem. Eng. J. 377 (2019) 120123, https://doi.org/10.1016/j.cej.2018.10.060.
[31] N.F. Bastos Rebelo, K.A. Andreassen, L.I. Suarez Ríos, J.C. Piquero Camblor, H. J. Zander, C.A. Grande, Pressure drop and heat transfer properties of cubic isoreticular foams, Chem. Eng. Process. - Process Intensif. 127 (2018) 36–42, https://doi.org/10.1016/j.cep.2018.03.008.
[32] A. Lind, Ø. Vistad, M.F. Sunding, K.A. Andreassen, J.H. Cavka, C.A. Grande, Multipurpose structured catalysts designed and manufactured by 3D printing, Mater. Des. 187 (2020) 1–8, https://doi.org/10.1016/j.matdes.2019.108377.
[33] S. Danaci, L. Protasova, F. Snijkers, W. Bouwen, A. Bengaouer, P. Marty, Innovative 3D-manufacture of structured copper supports post-coated with catalytic material for CO2 methanation, Chem. Eng. Process. - Process Intensif. 127 (2018) 168–177, https://doi.org/10.1016/j.cep.2018.03.023.
[34] L. Fratalocchi, G. Groppi, C.G. Visconti, L. Lietti, E. Tronconi, Adoption of 3D printed highly conductive periodic open cellular structures as an effective solution to enhance the heat transfer performances of compact Fischer-Tropsch fixed-bed reactors, Chem. Eng. J. 386 (2020) 123988, https://doi.org/10.1016/j.cej.2019.123988.
[35] M. Ambrosetti, G. Groppi, W. Schwieger, E. Tronconi, H. Freund, Packed periodic open cellular structures - an option for the intensification of non-adiabatic catalytic processes, Chem. Eng. Process. - Process Intensif. (2020), https://doi.org/10.1016/j.cep.2020.108057.
[36] L. Wang, M. Gandorfer, T. Selvam, W. Schwieger, Determination of faujasite-type zeolite thermal conductivity from measurements on porous composites by laser flash method, Mater. Lett. 221 (2018) 322–325, https://doi.org/10.1016/j.matlet.2018.03.157.
[37] L. Turchetti, M.A. Murmura, G. Monteleone, M.C. Annesini, Wall heat transfer coefficient and effective radial conductivity of ceramic foam catalyst supports, Chem. Eng. Res. Des. 156 (2020) 146–155, https://doi.org/10.1016/j.cherd.2020.01.021.
[38] X. Fan, X. Ou, F. Xing, G.A. Turley, P. Denissenko, M.A. Williams, N. Batail, C. Pham, A.A. Lapkin, Microtomography-based numerical simulations of heat transfer and fluid flow through β-SiC open-cell foams for catalysis, Catal. Today 278 (2016) 350–360, https://doi.org/10.1016/j.cattod.2015.12.012.
[39] E. Bianchi, T. Heidig, C.G. Visconti, G. Groppi, H. Freund, E. Tronconi, An appraisal of the heat transfer properties of metallic open-cell foams for strongly exo-/endothermic catalytic processes in tubular reactors, Chem. Eng. J. 198–199 (2012) 512–528, https://doi.org/10.1016/j.cej.2012.05.045.
[40] J. Randrianalisoa, D. Baillis, C.L. Martin, R. Dendievel, Microstructure effects on thermal conductivity of open-cell foams generated from the Laguerre–Voronoï tessellation method, Int. J. Therm. Sci. 98 (2015) 277–286, https://doi.org/10.1016/j.ijthermalsci.2015.07.016.
[41] M. Bracconi, M. Ambrosetti, M. Maestri, G. Groppi, E. Tronconi, A systematic procedure for the virtual reconstruction of open-cell foams, Chem. Eng. J. 315 (2017), https://doi.org/10.1016/j.cej.2017.01.069.
[42] E. Bianchi, W. Schwieger, H.H. Freund, Assessment of Periodic Open Cellular Structures for Enhanced Heat Conduction in Catalytic Fixed-Bed Reactors, Adv. Eng. Mater. 18 (n.d.) 608–614. doi:10.1002/adem.201500356.
[43] V. Balakotaiah, Z. Sun, D.H. West, Autothermal reactor design for catalytic partial oxidations, Chem. Eng. J. 374 (2019) 1403–1419, https://doi.org/10.1016/j.cej.2019.05.155.
[44] M. Klumpp, A. Inayat, J. Schwerdtfeger, C. Körner, R.F. Singer, H. Freund, W. Schwieger, Periodic open cellular structures with ideal cubic cell geometry: effect of porosity and cell orientation on pressure drop behavior, Chem. Eng. J. 242 (2014) 364–378, https://doi.org/10.1016/j.cej.2013.12.060.
[45] H.G. Weller, G. Tabor, H. Jasak, C. Fureby, A Tensorial Approach to Computational Continuum Mechanics Using Object-oriented Techniques, 1998, p. 12.
[46] M. Ambrosetti, M. Bracconi, G. Groppi, E. Tronconi, Analytical geometrical model of open cell foams with detailed description of strut-node intersection, Chemie-Ingenieur-Technik. 89 (2017), https://doi.org/10.1002/cite.201600173.
[47] J.C. Maxwell, A Treatise on Electricity and Magnetism, 3rd edition, 1892. Oxford.
[48] R. Lemlich, A theory for the limiting conductivity of polyhedral foam at low density, J. Colloid Interface Sci. 64 (1978) 107–110. https://doi.org/10.1016/0021-9797(78)90339-9.
[49] H.A.J. Van Dijk, J. Boon, R.N. Nyqvist, R.W. Van Den Brink, Development of a single stage heat integrated water – gas shift reactor for fuel processing, Chem. Eng. J. 159 (2010) 182–189, https://doi.org/10.1016/j.cej.2010.02.046.
[50] C.G. Visconti, G. Groppi, E. Tronconi, Accurate prediction of the effective radial conductivity of highly conductive honeycomb monoliths with square channels, Chem. Eng. J. 223 (2013) 224–230, https://doi.org/10.1016/j.cej.2013.02.095.